water

MDPI

Article

Experimental Study on the Sedimentation Characteristics of Classified Tailings Underwater

Ke Qin [1,2,3,*], Jiewang Gao [2,3], Xiaogang Wu [2,3], Kai Tang [2,3], Minghua Luo [2,3], Yunlong Shu [2,3,4] and Keliang Xiao [2,3]

[1] School of Eco-Environment and Chemical Engineering, Xi'an University of Technology, Xi'an 710048, China
[2] Sinosteel Maanshan Institute of Mining Research Co., Ltd., Maanshan 243000, China; gjw18170400061@163.com (J.G.); gisluo@outlook.com (M.L.); yunlong_shu@163.com (Y.S.)
[3] State Key Laboratory of Metal Mine Mining Safety and Disaster Prevention and Control, Maanshan 243000, China
[4] School of Resource Environment and Safety Engineering, University of South China, Hengyang 421001, China
* Correspondence: zhonggangqinke@yeah.net

Abstract

Understanding the short-term underwater settling behavior of classified tailings is important for interpreting deposit formation in ponded areas. One-dimensional settling-column tests were conducted for 36 h to examine how fine-particle content (<0.075 mm) and nominal slurry mass concentration were associated with soil-water interface evolution, visually defined settling phases, and cumulative interface displacement. The observations showed an early rapid-settling period, a post-interface settling/compression period, and a later low-rate compression period. After 36 h, the columns displayed a clear-water zone above a visually layered deposit. Across the six treatment means, 36 h cumulative settlement decreased as fine-particle content or nominal mass concentration increased. These are time-specific descriptive trends, not evidence of lower ultimate settlement: equilibrium was not demonstrated, only duplicate runs were performed, and the archived concentration-series records do not contain the run-specific initial volume, height, or component masses needed to isolate a concentration effect. No rheological, pore-pressure, microstructural, strength, or water-content measurements were made. The results therefore describe short-term behavior in a static laboratory column and should not be directly extrapolated to field-scale tailings facilities.

Keywords: classified tailings; underwater settling; fine-particle content; slurry mass concentration; 36 h cumulative settlement; settling-column test

Check for updates

Academic Editor: Pedro Proença Cunha

Received: 14 July 2026
Revised: 19 August 2026
Accepted: 21 August 2026
Published: 27 August 2026

Copyright: © 2026 by the authors. Licensee MDPI, Basel, Switzerland. This article is an open access article distributed under the terms and conditions of the Creative Commons Attribution (CC BY) license.

1. Introduction

Tailings reservoirs are essential infrastructure for mine production [1,2], and their safe operation is closely related to ecological protection, public safety, and long-term risk management [3,4]. After hydraulic discharge into a reservoir, tailings undergo gravity- and flow-induced sorting. Coarse particles are deposited rapidly near the discharge point, whereas fine particles migrate with the slurry toward the distal ponded area, producing a sedimentary body with pronounced spatial heterogeneity [5–7]. According to beach morphology and reservoir topography, the deposition area can generally be divided into a dry beach section, a transition section, and an underwater sedimentary section (Figure 1). The dry beach section is a low-moisture zone above the pond water level, and its length is an important indicator of tailings reservoir operation and flood-control safety. The transition

section is the saturated zone between the dry beach and the ponded area, where tailings gradually change from an unsaturated to a saturated state. The underwater sedimentary section is located below the pond water level. With increasing distance from the discharge point, the deposited material gradually changes from sandy tailings to silty and clayey tailings, making this section the main enrichment area for fine-grained tailings.

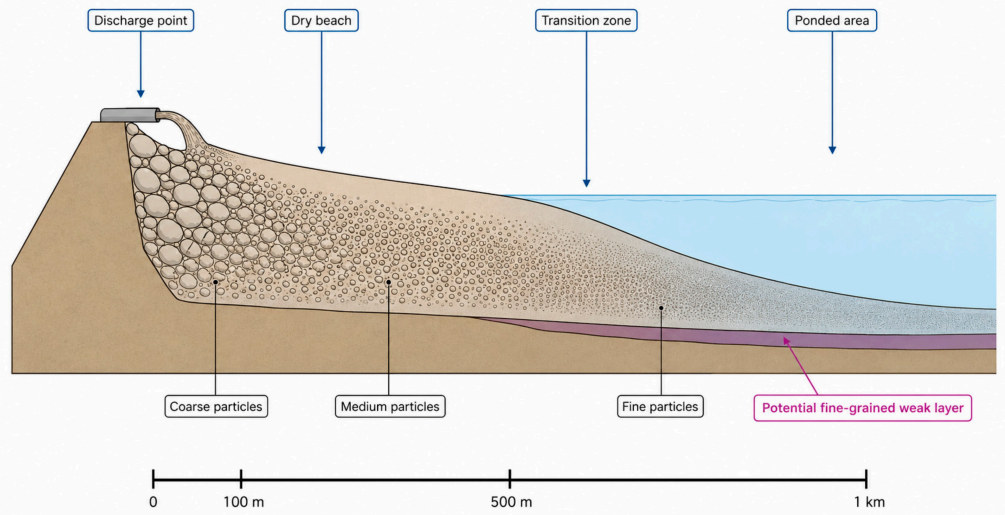

Figure 1. Conceptual cross-section of a tailings beach and ponded area. Particle size decreases with distance from the discharge point, and the potential fine-grained weak layer is shown at the distal pond bottom. The 0–1 km bar provides order-of-magnitude context only; zone widths are site-specific, the drawing is not to scale, and the layer location was not measured in the present column tests.

Once fine-grained tailings enter a ponded area, they may remain suspended for long periods because their settling velocity is low and particle interactions become important. Previous studies have reported that fine-grained tailings deposits can retain high water contents and exhibit low shear strength [8–11]. These literature-derived properties were not measured in the present tests. Existing studies have mainly focused on the physical and mechanical properties of tailings in dry beach areas, whereas quantitative observations of soil-water interface evolution in ponded, fine-grained tailings remain limited. Compared with sediment-laden flow in natural rivers, tailings slurry commonly has a higher solids concentration, lower flow velocity, and a larger fraction of fine particles, so its settling behavior cannot be inferred directly from river-sediment analogies [12–15].

This study used one-dimensional settling-column tests to document the 36 h underwater settling response of classified tailings under different fine-particle contents and nominal slurry mass concentrations. The protocol was informed by earlier static settling-column studies of tailings [16–18]; those references support the choice of method, not the present results. Classical descriptions of particle settling and low-Reynolds-number hydrodynamics provide additional background for interpreting sedimentation behavior [19–21]. Tailings-dam design and failure studies further highlight the engineering significance of deposition and storage behavior [22–24]. The objectives were to quantify interface appearance time, cumulative interface displacement, and settling rate; to define phase boundaries using observable criteria; and to identify the limits of short-duration static-column evidence. The work was designed as a descriptive laboratory investigation rather than a predictive model or field-scale simulation.

2. Materials and Methods

The experimental basis was a controlled, one-dimensional static settling-column comparison. One factor was varied at a time while the other was held fixed, and the response

was defined by the observed soil-water interface. The design was intended to describe short-term interface kinetics, not to validate a particle-scale predictive model. Sample preparation, apparatus, operation, and the operational phase criteria are specified below.

2.1. Tailings Characterization and Sample Preparation

The classified tailings used in this study were obtained from a typical metal mine tailings pond in China. Their basic physical and chemical properties were tested according to national standards, providing a basis for subsequent experimental analysis. The main mineral components were quartz, feldspar, and clay minerals, and the specific gravity was 2.65–2.70. The initial moisture content of the as-received tailings was 15.2 ± 0.5%, and the pore water was weakly alkaline (pH = 7.8–8.2) with low salinity. In accordance with the Standard for Geotechnical Test Methods (GB/T 50123-2019) [25] and the Code for Design of Tailings Facilities (GB 50863-2013) [26], particles smaller than 0.075 mm are defined as fine particles. Tailings are classified into sandy, silty, and clayey categories according to particle gradation and plasticity index, with the classification criteria shown in Table 1. Naming was prioritized by particle gradation from coarse to fine in accordance with the classification standards, and the plasticity index was calculated from the liquid limit measured when a 76 g cone penetrated 10 mm into the soil.

Table 1. Tailings classification table.

Tailings Category	Tailings Name	Classification Criteria
Sandy Tailings	Tailings Gravelly Sand	Particles larger than 2 mm account for 25–50% of the total mass
	Tailings Coarse Sand	Particles larger than 0.5 mm account for more than 50% of the total mass
	Tailings Medium Sand	Particles larger than 0.25 mm account for more than 50% of the total mass
	Tailings Fine Sand	Particles larger than 0.074 mm account for more than 85% of the total mass
	Tailings Silty Sand	Particles larger than 0.074 mm account for more than 50% of the total mass
Silty Tailings	Tailings Silty Soil	Particles larger than 0.074 mm account for no more than 50% of the total mass, and the plasticity index is ≤10
Clayey Tailings	Tailings Silty Clay	Plasticity index > 10 and ≤17,Plasticity index > 17
	Tailings Clay	

Note(s): Naming shall be determined according to particle gradation from large to small, based on the first matching criterion. The plasticity index shall be calculated from the liquid limit measured when a 76 g cone penetrates the soil to a depth of 10 mm.

To quantify the particle size effect, particle gradation analysis was carried out on tailings samples with different fine particle contents, and key parameters such as effective particle size d_{10}, median particle size d_{30}, average particle size d_{50} and limiting particle size d_{60} were measured. The main characteristics (gradation index) of the particle size distribution curve can be reflected by the uniformity coefficient C_u and curvature coefficient C_c [27–29].

$$C_u = \frac{d_{60}}{d_{10}} \quad (1)$$

$$C_c = \frac{d_{30}^2}{d_{60} \times d_{10}} \quad (2)$$

where C_u reflects the uniformity of particle gradation. The smaller C_u is, the more uniform the gradation is. Tailings with $C_u \geq 5$ and C_c = 1~3 are easier to compact. The gradation parameters of tailings with different fine particle contents are shown in Table 2. It can be seen from the table that with the increase of fine particle content, d_{10} decreases from 0.090 mm to 0.0053 mm, and C_u first increases to 15.696 (40% fine particle content) and then gradually decreases [30,31], indicating that fine particle content significantly changes the particle size distribution characteristics of tailings, thereby affecting their sedimentation and consolidation behavior. The particle gradation curves of tailings with different fine particle contents are shown in Figure 2, which intuitively reflects the difference law of particle size distribution.

Table 2. Boundary coefficient and particle size parameters of tailings with different fine particle contents.

Fine Particle Content (<0.075 mm)	Boundary Particle Size				Boundary Coefficients	
	Effective Size (d10)	Median Size (d30)	Mean Size (d50)	Limiting Size (d60)	Uniformity Coefficient (Cu)	Curvature Coefficient (Cc)
--	mm	mm	mm	mm	--	--
0	0.090	0.125	0.162	0.183	2.033	0.949
20	0.024	0.092	0.141	0.156	6.500	2.261
40	0.0079	0.057	0.096	0.124	15.696	3.317
60	0.0068	0.022	0.064	0.076	11.176	0.937
80	0.0060	0.012	0.042	0.058	9.667	0.414
100	0.0053	0.0087	0.023	0.037	6.981	0.386

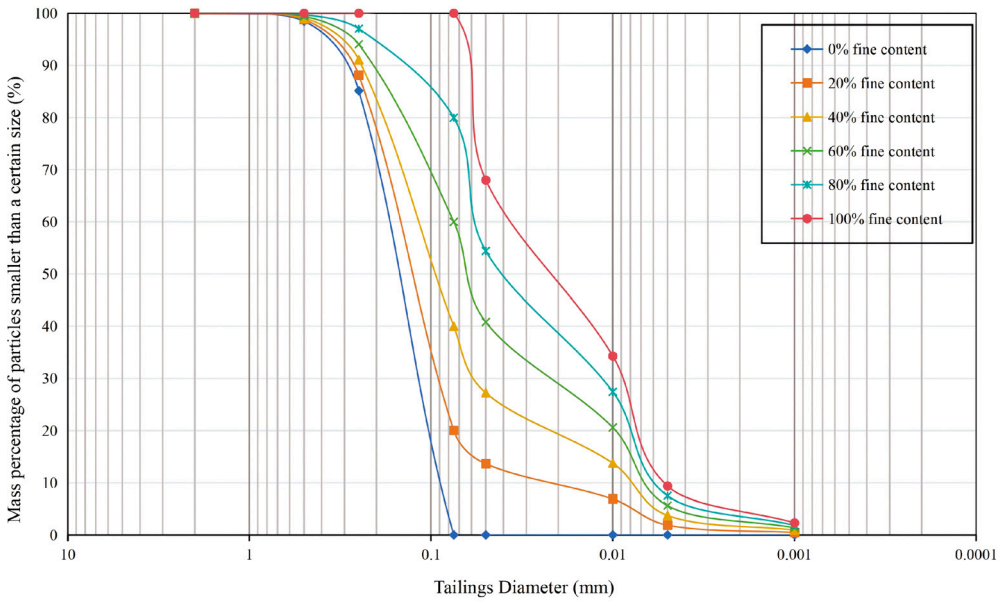

Figure 2. Particle analysis curves of tailings with different fine particle (<0.075 mm) contents.

To prepare gradient samples with fine-particle contents of 0–100% and ensure test comparability, precise mass proportioning was performed for each particle-size interval: 2–0.5 mm, 0.5–0.25 mm, 0.25–0.075 mm, and less than 0.075 mm. The specific proportioning data are shown in Table 3. Samples were prepared strictly according to the designed proportions to ensure that the particle-size distributions met the test requirements [28–31].

Table 3. Proportioning table of fine particle (<0.075 mm) content for different tailings particle size effects.

Particle Size (mm) Content (<0.075 mm)/g	2~0.5	0.5~0.25	0.25~0.075	0.075~0.05	0.05~0.01	0.01~0.005	0.005~0.001	<0.001
0	1.53	13.36	85.11	0.00	0.00	0.00	0.00	0.00
20	1.22	10.69	68.09	6.40	6.75	4.99	1.41	0.46
40	0.92	8.02	51.07	12.79	13.50	9.97	2.82	0.92
60	0.61	5.34	34.05	19.19	20.24	14.96	4.23	1.38
80	0.31	2.67	17.02	25.58	26.99	19.95	5.64	1.84
100	0.00	0.00	0.00	31.98	33.74	24.93	7.05	2.30

2.2. Experimental Apparatus

The apparatus followed the static settling-column approach used in earlier tailings studies [16–18], with modifications for non-flocculated classified tailings. It consisted of a 5 L transparent acrylic cylinder with an inner diameter of 10 cm and a height of 65 cm. A vertical graduated strip with 1 mm resolution was attached to the outer wall so that the soil-water interface height could be read consistently. The same cylinder geometry, scale position, camera viewpoint, and observation schedule were used for all conditions. Because these dimensions and procedures fully define the apparatus used in this study, the former apparatus photograph was removed.

2.3. Experimental Design and Operation Process

Two groups of single-factor controlled tests were designed to separately examine the effects of fine-particle content and slurry mass concentration. The test scheme is shown in Table 4.

Table 4. Test scheme of one-dimensional sedimentation characteristics of tailings slurry.

No.	Group	Test Level (Mass %)
A	Content of particles <0.075 mm(Tailings slurry mass concentration = 20%)	0 20 40 60 80 100
B	Mass concentration of tailings slurry/%(Content of particles <0.075 mm = 40%)	10 20 30 40 50 60

Group A (particle-size effect test): The tailings slurry mass concentration was fixed at 20%, and the fine-particle content (<0.075 mm) was set at six levels: 0%, 20%, 40%, 60%, 80%, and 100%.

Group B (mass-concentration effect test): The fine-particle content was fixed at 40%, and the tailings slurry mass concentration was set at six levels: 10%, 20%, 30%, 40%, 50%, and 60%.

The tests were conducted in accordance with the Standard for Geotechnical Test Methods, and the procedure was as follows:

1. The corresponding masses of tailings and deionized water were weighed according to the test scheme and placed in a stirring container.

2. The mixture was stirred with an electric mixer for 2 h to fully disperse the tailings particles in water and form a uniform suspension, thereby avoiding particle segregation before testing.
3. The uniformly mixed tailings slurry was slowly injected into the sedimentation column and manually stirred for 30 s after injection to eliminate local concentration differences.
4. The soil-water interface height was recorded at preset times (0 s, 30 s, 60 s, 90 s, 120 s, 3 min, 5 min, 8 min, 12 min, 17 min, 25 min, 35 min, 50 min, 1.5 h, 2.5 h, 4 h, 6 h, 9 h, 18 h, and 36 h). The interpretation of the settling and compression processes was informed by previous studies on self-weight consolidation, one-dimensional consolidation, and fine-tailings flocculation [32–34]. Cumulative settlement was calculated as $s(t) = h0 - h(t)$, where h0 is the initial interface height and h(t) is the interface height at time t [16,35,36]. The operational interpretation was also informed by established concepts of sedimentation and thickening [37].

All tests were conducted at 20 ± 1 degrees C with deionized water and without polymeric flocculant. The system remained static and free from external vibration. Each condition was repeated twice, and the manuscript reports the mean of the two runs. The retained dataset contains treatment means but not the individual time histories, so replicate-level standard deviations, confidence intervals, and error bars cannot be reconstructed. The duplicate design and the absence of replicate-level variability limit statistical inference and are acknowledged in Section 4.2. Slurry mass concentration was defined on a wet-mass basis as $C_m = \frac{m_s}{m_s+m_w} \times 100\%$, where m_s is the oven-dry equivalent mass of tailings and m_w is the mass of deionized water. The archived records used for this revision do not contain run-specific m_s, m_w, initial slurry volume, or initial fill height. Absolute displacements in the concentration series therefore describe the tested conditions but do not isolate concentration as a causal variable. The three phases were defined operationally. The end of the early rapid-settling period was the first scheduled observation at which a continuous soil-water interface could be identified visually. The onset of the low-rate compression period was the first scheduled observation for which the finite-difference interface-displacement rate was below 0.01 cm/h and remained below that threshold for the subsequent recorded intervals. The threshold of 0.01 cm/h was used as a pragmatic operational criterion to identify a sustained low-rate regime within the available observation schedule. It is not intended to represent a universal physical boundary between settling and consolidation mechanisms. The intervening period was termed post-interface settling/compression. These labels do not imply classical primary or secondary consolidation because pore-water pressure was not measured.

3. Results

3.1. Phenomenological Observation of Sedimentation Mode

The settling columns showed visually distinct modes of particle motion. For descriptive purposes, the observations were grouped as rapid individual-particle settling, settling of floc-like aggregates, collective settling of network-like aggregates, and mixed settling. These categories are based on interface appearance and photographs only; they do not establish floc structure, pore geometry, water content, void ratio, strength, or particle-size stratification. The visual characteristics are summarized in Table 5.

Table 5. Classification of slurry sedimentation characteristics.

Deposition Type	Free Deposition	Floc Deposition	Floc-Network Deposition	Mixed Deposition
Soil–water interface	Forms instantaneously and is clear	Unclear at early settling stage	Becomes clear rapidly	Depends on sand content
Deposition Characteristics	Coarse particles settle individually; no flocs	Small and independent flocs	Flocs interconnect to form a floc-network structure	Individual particles and flocculated structures

The observed morphology is shown in Figure 3. The descriptions below refer only to features visible during the test.

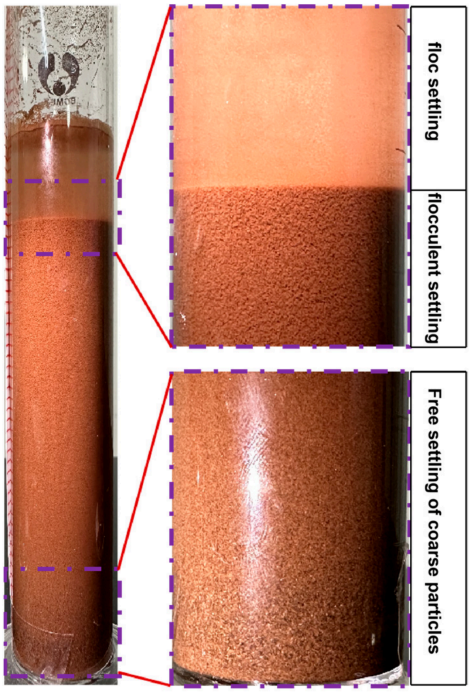

Figure 3. Visual examples of settling modes observed in the columns.

(1) Rapid individual-particle settling: Coarser particles (>0.075 mm) descended rapidly and accumulated at the base. Depending on fine-particle content, a continuous soil-water interface first became visible between 1.5 and 90 min.
(2) Settling of floc-like aggregates: Fine particles (<0.075 mm) remained suspended longer, and small aggregate-like features were visible. No polymeric flocculant was added. Electrical double-layer interactions, colloidal attraction, and network formation are possible explanations from the literature [38–40], but they were not measured in this study.
(3) Collective settling of network-like aggregates: At later times, aggregate-like features appeared to connect and descend collectively, and the interface became easier to identify. The photographs support this morphological description only.

After 36 h, the columns displayed a clear-water zone above a visually layered deposit (Figure 4). The term 'layered' refers to differences in appearance in the photographs; the layers were not sampled for water content, particle-size distribution, void ratio, strength, or microstructure. Because equilibrium was not demonstrated, the 36 h profile should not be described as a final or stable state.

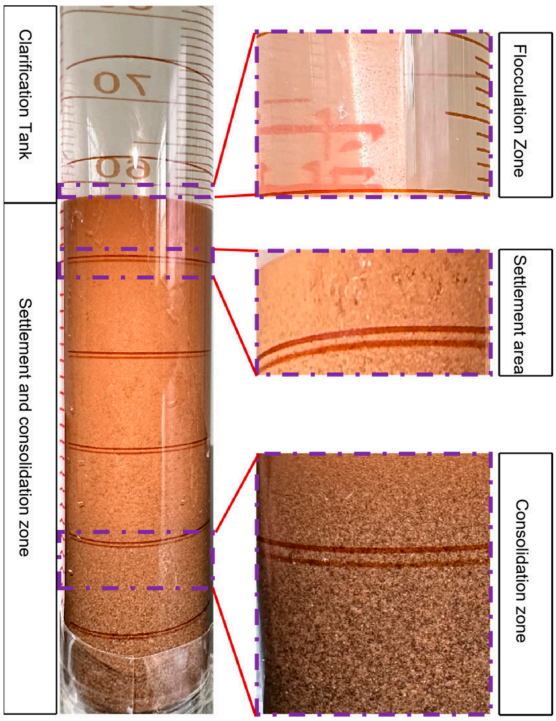

Figure 4. Visual layering after 36 h. Zone labels are based on appearance only and do not indicate measured material-property boundaries.

(1) Clear-water zone: The region above the visible interface. More suspended material remained visible in tests with higher fine-particle content.
(2) Upper aggregate-rich zone: A loose, floc-like layer immediately below the interface, identified visually.
(3) Intermediate settling zone: A region with a more continuous appearance than the upper aggregate-rich zone. No pore-channel dimensions were measured.
(4) Lower compacted zone: The visually denser region near the base. No claim is made about water content, microcracking, shear strength, or vertical particle-size distribution.

3.2. Influence of Particle Size Effect (Fine Particle Content)

Table 6 summarizes the descriptive outcomes for the six fine-particle-content conditions.

Table 6. Record table of sedimentation and consolidation test results under different tailings particle size effects.

Fine-Particle Content (<0.075 mm)	Interface-Formation Time	Settlement During Rapid-Settling Period	Mean Rate During Rapid-Settling Period	Onset of Low-Rate Compression	36 h Cumulative Settlement
--	min	cm	cm/min	min	cm
0	1.5	9.8	6.53	25	10.03
20	8	8.43	1.05	150	9.94
40	25	7.92	0.32	240	8.97
60	35	7.45	0.21	240	8.55
80	42.5	7.5	0.18	150	8.41
100	90	7.95	0.09	150	7.98

3.2.1. Sedimentation Rate and Soil-Water Interface Characteristics

Across the treatment means, a larger fine-particle content was associated with later interface appearance and a lower mean rate during the rapid-settling period. The interface

appeared at 1.5 min for 0% fine particles and at 90 min for 100% fine particles; the corresponding mean rates were 6.53 and 0.09 cm/min. The tests did not measure the colloidal or rheological variables needed to identify the mechanism, so the trend is reported as an observation rather than attributed to a specific interaction.

3.2.2. Operationally Defined Settling Phases Under Different Fine-Particle Contents

The time intervals were assigned from two directly observable boundaries defined in Section 2.3 (Figure 5): (i) the first scheduled observation at which a continuous soil-water interface could be identified and (ii) the first scheduled observation at which the finite-difference displacement rate fell below 0.01 cm/h and remained below that threshold thereafter. Figure 5 maps those recorded boundaries on a logarithmic time axis. No boundary was inferred between scheduled readings, and the terms do not imply classical primary or secondary consolidation without pore-pressure measurements.

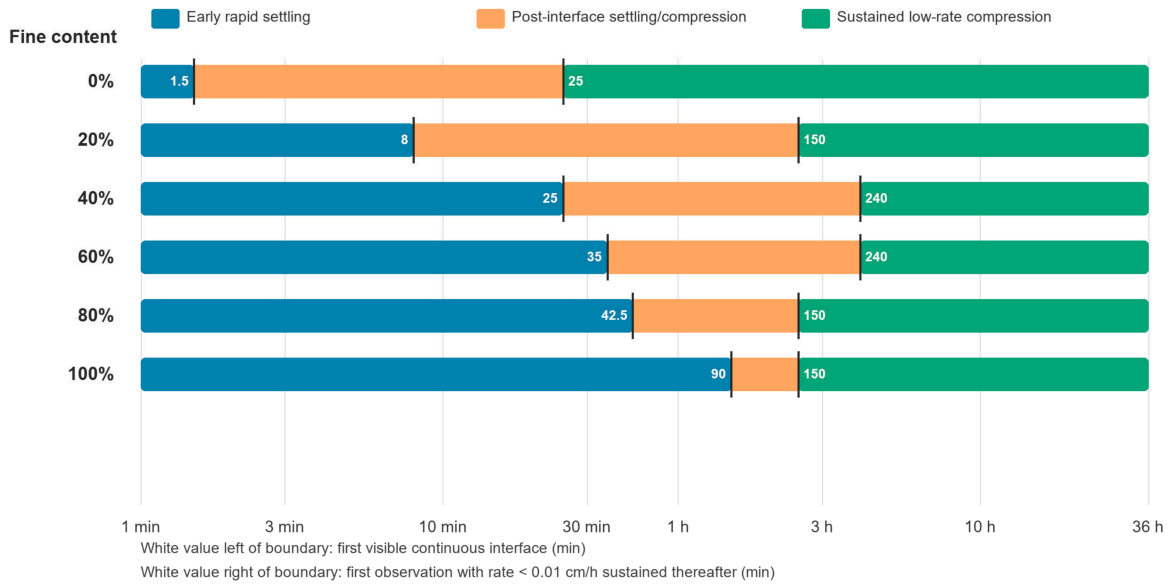

Figure 5. Operational phase timing for the fine-particle-content series. Boundary labels are scheduled observation times in minutes. The second boundary is the first observation with a finite-difference displacement rate below 0.01 cm/h that remained below the threshold thereafter; no interpolation or pore-pressure criterion was used.

Early rapid-settling period: The interface, when visible, descended rapidly and most of the 36 h displacement accumulated during this interval.

Post-interface settling/compression period: After a continuous interface formed, its descent slowed. The data do not distinguish continued hindered settling from drainage-controlled compression.

Low-rate compression period: The finite-difference interface-displacement rate was below 0.01 cm/h and remained below this threshold for subsequent observations.

The first boundary increased from 1.5 min at 0% fine particles to 90 min at 100%. The second boundary occurred between 25 and 240 min across the conditions. These observation-time breakpoints should therefore be interpreted as reproducible classification points for the present dataset rather than intrinsic material transition times, and they do not represent pore-pressure dissipation or completion of consolidation.

3.2.3. Descriptive Relationship of 36 h Cumulative Settlement with Fine-Particle Content

A linear function and a two-parameter exponential function were fitted to the six treatment means to test whether the apparent 36 h trend required a nonlinear description (Figure 6):

$$\text{Linear: } s36 = 10.0700 - 0.02180\,m$$

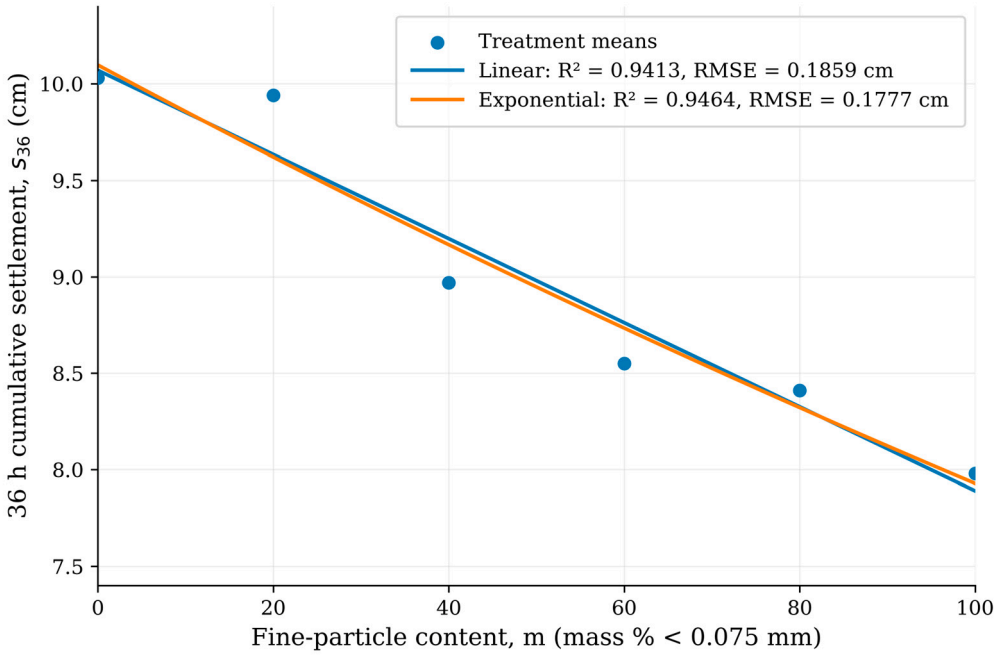

Figure 6. Comparison of linear and exponential descriptions of 36 h cumulative settlement versus fine-particle content. Points are the six treatment means. The curves are empirical sensitivity checks, not constitutive relationships or predictions of ultimate settlement.

Exponential: $s36 = 10.0975 \exp(-0.002418m)$, where s36 is 36 h cumulative settlement (cm), and m is fine-particle content in mass percentage points.

The exponential fit was only marginally closer to the six means (R^2 = 0.9464, RMSE = 0.1777 cm, AICc = −12.74) than the linear fit (R^2 = 0.9413, RMSE = 0.1859 cm, AICc = −12.19). The AICc difference of 0.54 is too small to distinguish the two empirical forms. The linear slope therefore remains a local summary of the tested interval, while the exponential curve shows that a plausible nonlinear form gives essentially the same conclusion. Neither fit establishes a general law or ultimate compressibility.

3.3. Response Under Different Nominal Slurry Mass Concentrations

Table 7 summarizes the descriptive outcomes for the six nominal mass-concentration conditions. Because run-specific component masses and initial geometry are absent from the archived dataset, comparisons of absolute displacement cannot isolate concentration as the causal factor.

Table 7. Record table of sedimentation and consolidation test results under different tailings mass concentrations.

Slurry Mass Concentration	Interface-Formation Time	Settlement During Rapid-Settling Period	Mean Rate During Rapid-Settling Period	Onset of Low-Rate Compression	36 h Cumulative Settlement
--	min	cm	cm/min	min	cm
10	5	16.2	3.24	17	16.43
20	12	13.7	1.14	50	15.57
30	35	6.78	0.19	240	10.97
40	50	7.47	0.15	360	10.52
50	90	6.38	0.07	360	8.76
60	150	5.91	0.04	540	6.53

3.3.1. Interface Appearance and Settling Rate

Across the tested condition means, interface appearance was later, and the mean rapid-settling rate was lower at higher nominal mass concentration. The rate decreased from 3.24 cm/min at 10% to 0.04 cm/min at 60%, while interface appearance shifted from 5 to 150 min. Increased hindered settling or rheological resistance is consistent with suspension-settling literature, but viscosity, rheology, ionic strength, conductivity, and floc-size distribution were not measured here. These mechanisms are therefore hypotheses rather than experimental findings.

3.3.2. Operationally Defined Settling Phases Under Different Slurry Mass Concentrations

The same two observable boundaries were applied to the nominal concentration series (Figure 7): first appearance of a continuous interface and first sustained finite-difference rate below 0.01 cm/h.

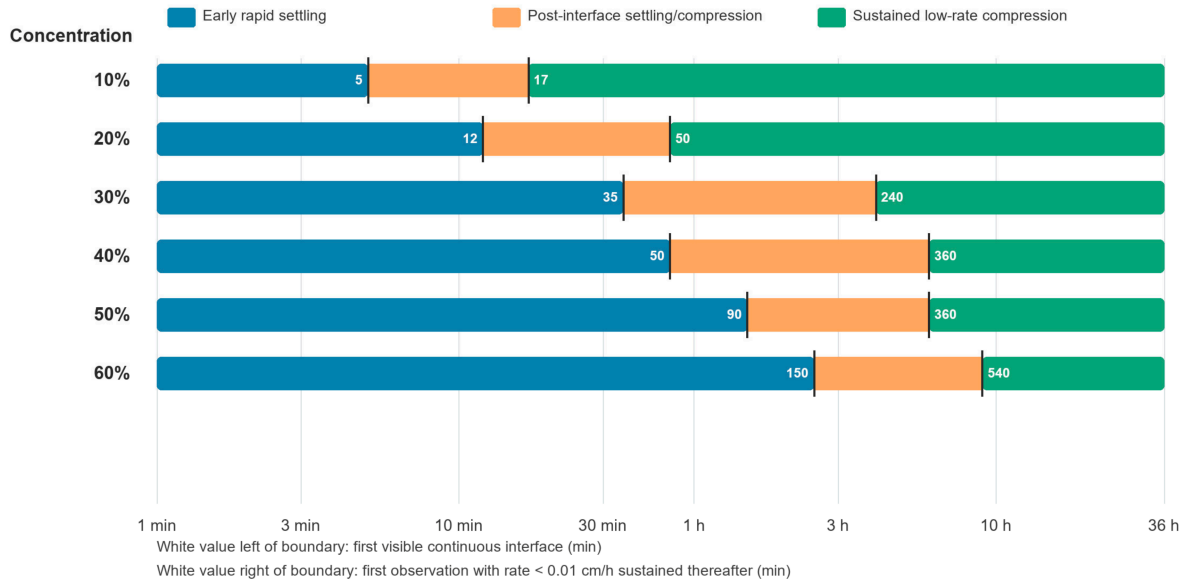

Figure 7. Operational phase timing for the nominal slurry mass-concentration series. Boundary labels are scheduled observation times in minutes, using the same interface-visibility and sustained-rate criteria as Figure 5.

The onset of sustained low-rate compression shifted from 17 min at 10% nominal mass concentration to 540 min at 60%. This observation is consistent with slower settling or drainage at higher solids loading, but it does not demonstrate excess pore-water-pressure dissipation because pore pressure and permeability were not measured.

3.3.3. Descriptive Relationship of 36 h Cumulative Settlement with Slurry Mass Concentration

An ordinary least-squares line was fitted to the six treatment means to summarize the 36 h trend (Figure 8):

$$s36 = 18.5013 - 0.20109c$$

where s36 is 36 h cumulative settlement (cm), and c is nominal slurry mass concentration in percentage points.

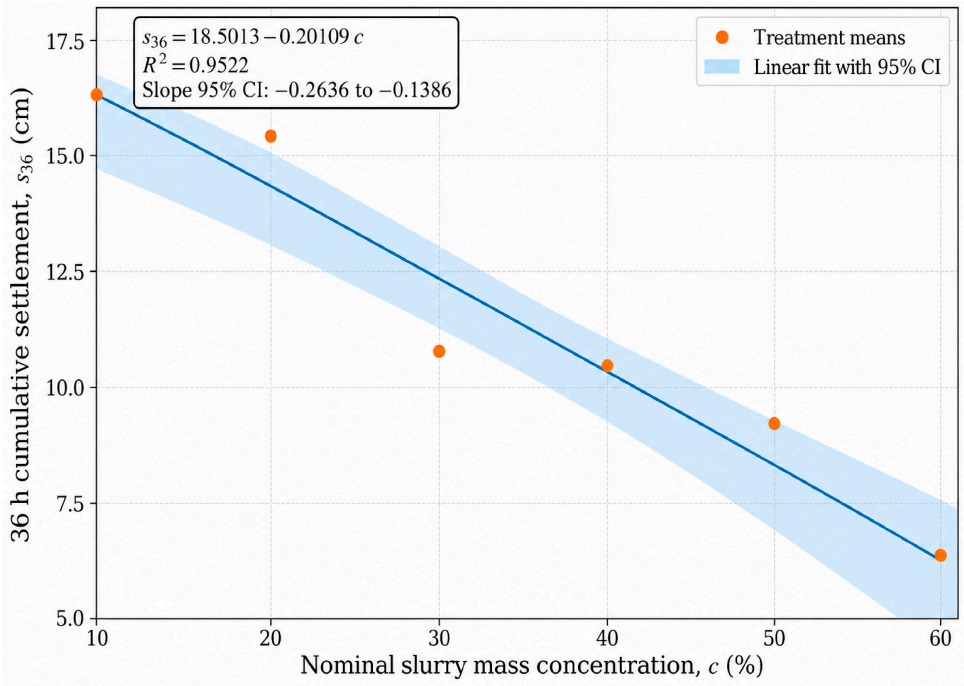

Figure 8. Descriptive ordinary least-squares fit between nominal slurry mass concentration and 36 h cumulative settlement. The shaded band is the 95% confidence band for the fitted mean across six treatment means; it is not replicate-level uncertainty.

The fitted slope was −0.20109 cm per percentage point (95% CI −0.26361 to −0.13857; R^2 = 0.9522). This regression summarizes the six condition means only. It does not isolate concentration from differences in initial solids mass or geometry, and it does not establish a smaller long-term settlement. The lower 36 h displacement at higher nominal concentration may reflect a slower approach to equilibrium.

4. Discussion

4.1. Interpretation of the Time-Specific Trends

The most defensible result is kinetic: within 36 h, columns with more fine particles or higher nominal mass concentration generally showed later interface formation and slower interface movement. Increasing the fine fraction decreases characteristic particle size and free-settling velocity, increases specific surface area and the opportunity for particle interactions, and can reduce the permeability of the accumulating deposit. In a concentrated suspension, those changes alter hindered-settling flux and drainage time [12–15,41,42]. Thus, less displacement at 36 h can arise from slower settling and drainage even if the deposit remains compressible. A smooth nonlinear relation is physically plausible outside the tested interval, but six treatment means over a fixed observation window cannot identify a power-law exponent, an exponential asymptote, or ultimate settlement.

The aggregate-like structures in the photographs are consistent with colloidal attraction or electrical double-layer effects discussed in the literature [38–40]. No polymer was

added, however, and no zeta potential, ionic strength, conductivity, aggregate-size distribution, rheology, or microstructure was measured. The term 'floc-like' is consequently used as a visual descriptor rather than proof of a specific aggregation mechanism.

4.2. Evidence and Uncertainty

The experiment has three important evidentiary limits. First, each condition was duplicated rather than independently replicated at least three times, and only treatment means are retained; replicate variability and inferential statistics cannot be reconstructed. Second, the archived concentration-series records lack run-specific component masses and initial slurry geometry, so absolute displacement does not isolate the concentration effect. Third, the 36 h endpoint was not tied to an equilibrium criterion. The regressions and phase times should therefore be read as descriptive summaries of the tested columns, not general material laws.

The study also measured only interface height and visual appearance. Water content, void ratio, shear strength, drainage-channel size, permeability, pore pressure, microcracking, rheology, and vertical particle-size distribution were not measured. Claims requiring those measurements have been removed. Single-particle force-balance treatments [19–21,43] are also insufficient for the concentrated suspensions tested here because they do not represent concentration-wave propagation, solids flux, permeability-porosity coupling, compressive yield stress, or pore-fluid drainage. For this reason, the unvalidated model and its equations were removed rather than presented as predictive.

4.3. Applicability to Tailings Facilities

The 10 cm diameter static column provides a controlled comparison of short-term vertical settling under hydrostatic laboratory conditions. It does not reproduce continuous discharge, horizontal advection, beach-slope sorting, repeated deposition, field drainage boundaries, seepage, evaporation, spatial heterogeneity, or scale effects. Field geophysical studies at an operational tailings facility have mapped laterally and vertically variable facies, the water table and saturation state, and depth-dependent elastic properties [44,45]. That evidence shows that real tailings stratigraphy is a three-dimensional, history-dependent system rather than a scaled-up settling column. Direct use of the reported displacements for dam-stability calculations, discharge management, post-construction settlement prediction, or closure design is therefore not justified.

The observations can instead serve as a screening-scale basis for selecting mixtures and observation intervals for longer tests. Transfer to an operating facility would require: (i) equilibrium-controlled column or large-cell tests with at least three independent replicates and complete mass and geometry records; (ii) pore-pressure, permeability, rheology, and layer-sampling measurements; and (iii) validation against boreholes, cone penetration data, and/or geophysical facies and saturation profiles such as those demonstrated by Mollehuara-Canales et al. [44,45]. Agreement should be assessed for phase timing, vertical gradation, water-table position, and compressibility before any design use.

5. Conclusions

This study documented the 36 h settling response of classified tailings in one-dimensional static columns under different fine-particle contents and nominal slurry mass concentrations. The conclusions are restricted to the measurements and observation window used in the study:

(1) The columns showed an early rapid-settling period, a post-interface settling/compression period, and a later low-rate compression period. These phases were defined by interface visibility and a sustained rate threshold, not by pore-pressure dissipation.

After 36 h, a clear-water zone and visually distinct deposit zones were present, but equilibrium and layer properties were not established.

(2) Across the six fine-particle-content treatment means, interface formation was later, rapid-settling rates were lower, and 36 h cumulative settlement decreased as fine-particle content increased. A two-parameter exponential curve fitted the six means only marginally better than a line, so the dataset does not distinguish a nonlinear law. The physical interpretation is delayed settling and drainage within the fixed 36 h window, not reduced ultimate compressibility.

(3) Across the six nominal concentration treatment means, interface formation and the onset of low-rate compression were delayed at higher nominal concentration, and 36 h cumulative settlement decreased. Because run-specific initial mass, volume, and height are unavailable, these absolute displacements do not isolate a concentration effect or establish long-term settlement.

(4) The findings apply only to short-duration vertical settling in a static 10 cm diameter laboratory column. Field-scale interpretation requires longer equilibrium-controlled tests, additional replication, complete initial-condition records, pore-pressure and rheological measurements, layer sampling, and validation against representative stratigraphic, saturation, and geophysical profiles.

Author Contributions: K.Q. is the main author of the paper, providing the methodology, data, and materials for the paper; J.G. is one of the authors of the paper, contributing methodology, experiments, and data for the development of the paper; X.W. is one of the authors of the paper, providing methodology and experiments for the writing of the paper; K.T. is one of the authors of the paper, assisting in the implementation of the paper's experiments and collecting experimental data; M.L. helped with the revision and data processing of the paper; Y.S. completed the revision and editing of the paper; K.X. assisted in the data analysis of the paper. All authors have read and agreed to the published version of the manuscript.

Funding: This research was supported by Deep Earth Probe and Mineral Resources Exploration National Science and Technology Major Project (No. 2025ZD1010907).

Data Availability Statement: The raw data supporting the conclusions of this article will be made available by the authors upon reasonable request. Requests should be directed to the corresponding author, Ke Qin (zhonggangqinke@yeah.net).

Acknowledgments: The authors thank the handling editor and anonymous reviewers for comments that improved the manuscript.

Conflicts of Interest: Authors Ke Qin, Jiewang Gao, Xiaogang Wu, Kai Tang, Minghua Luo, Yunlong Shu and Keliang Xiao were employed by the company Sinosteel Maanshan Institute of Mining Research Co., Ltd. The authors declare that the research was conducted in the absence of any commercial or financial relationships that could be construed as a potential conflict of interest.

References

1. Kossoff, D.; Dubbin, W.E.; Alfredsson, M.; Edwards, S.J.; Macklin, M.G.; Hudson-Edwards, K.A. Mine Tailings Dams: Characteristics, Failure, Environmental Impacts, and Remediation. *Appl. Geochem.* **2014**, *51*, 229–245. [CrossRef]
2. Bussière, B. Colloquium 2004: Hydrogeotechnical Properties of Hard Rock Tailings from Metal Mines and Emerging Geoenvironmental Disposal Approaches. *Can. Geotech. J.* **2007**, *44*, 1019–1052. [CrossRef]
3. Roche, C.; Thygesen, K.; Baker, E. (Eds.) *Mine Tailings Storage: Safety Is No Accident: A UNEP Rapid Response Assessment*; United Nations Environment Programme: Nairobi, Kenya; GRID-Arendal: Arendal, Norway, 2017.
4. Global Tailings Review. *Global Industry Standard on Tailings Management*; International Council on Mining and Metals: London, UK; United Nations Environment Programme: Nairobi, Kenya; Principles for Responsible Investment: London, UK, 2020.
5. Fourie, A.B. Perceived and Realized Benefits of Paste and Thickened Tailings for Surface Deposition. *J. S. Afr. Inst. Min. Metall.* **2012**, *112*, 919–926.

6. Tian, S.; Zhao, Y.; Gong, Y. Experimental Study on Tailings Deposition Distribution Pattern and Sedimentation Characteristics. *ACS Omega* **2024**, *9*, 19428–19439. [CrossRef]
7. Wang, S.; Song, X.P.; Wang, X.J.; Chen, Q.S.; Qin, J.C.; Ke, Y.X. Influence of Coarse Tailings on Flocculation Settlement. *Int. J. Miner. Metall. Mater.* **2020**, *27*, 1065–1074. [CrossRef]
8. Wang, C.; Harbottle, D.; Liu, Q.; Xu, Z. Current State of Fine Mineral Tailings Treatment: A Critical Review on Theory and Practice. *Miner. Eng.* **2014**, *58*, 113–131. [CrossRef]
9. Landman, K.A.; White, L.R. Solid/Liquid Separation of Flocculated Suspensions. *Adv. Colloid Interface Sci.* **1994**, *51*, 175–246. [CrossRef]
10. Michaels, A.S.; Bolger, J.C. Settling Rates and Sediment Volumes of Flocculated Kaolin Suspensions. *Ind. Eng. Chem. Fundam.* **1962**, *1*, 24–33. [CrossRef]
11. Han, C.; Tan, Y.; Chu, L.; Song, W.; Yu, X. Flocculation and Settlement Characteristics of Ultrafine Tailings and Microscopic Characteristics of Flocs. *Minerals* **2022**, *12*, 221. [CrossRef]
12. Kynch, G.J. A Theory of Sedimentation. *Trans. Faraday Soc.* **1952**, *48*, 166–176. [CrossRef]
13. Richardson, J.F.; Zaki, W.N. Sedimentation and Fluidisation: Part I. *Chem. Eng. Res. Des.* **1997**, *75*, S82–S100. [CrossRef]
14. Buscall, R.; White, L.R. The Consolidation of Concentrated Suspensions. Part 1: The Theory of Sedimentation. *J. Chem. Soc. Faraday Trans. 1* **1987**, *83*, 873–891. [CrossRef]
15. Bürger, R.; Concha, F.; Fjelde, K.K.; Karlsen, K.H. Phenomenological Foundation and Mathematical Theory of Sedimentation-Consolidation Processes. *Chem. Eng. J.* **2000**, *80*, 177–188. [CrossRef]
16. Bian, J.; Wang, H.; Xiao, C.; Zhang, D. An Experimental Study on the Flocculating Settling of Unclassified Tailings. *PLoS ONE* **2018**, *13*, e0204230. [CrossRef]
17. Yin, S.; Hou, Y.; Yang, S.; Chen, X. Study on Static and Dynamic Flocculation Settlement Characteristics of Fine Tailings Slurry and Influence of Flocculant on Strength of Fine Tailings Backfill. *Case Stud. Constr. Mater.* **2022**, *17*, e01525. [CrossRef]
18. Wu, A.; Ruan, Z.; Bürger, R.; Yin, S.; Wang, J.; Wang, Y. Optimization of Flocculation and Settling Parameters of Tailings Slurry by Response Surface Methodology. *Miner. Eng.* **2020**, *156*, 106488. [CrossRef]
19. Happel, J.; Brenner, H. *Low Reynolds Number Hydrodynamics: With Special Applications to Particulate Media*; Martinus Nijhoff Publishers: The Hague, The Netherlands, 1983. [CrossRef]
20. Clift, R.; Grace, J.R.; Weber, M.E. *Bubbles, Drops, and Particles*; Academic Press: New York, NY, USA, 1978.
21. Dey, S. *Fluvial Hydrodynamics: Hydrodynamic and Sediment Transport Phenomena*; Springer: Berlin/Heidelberg, Germany, 2014. [CrossRef]
22. Vick, S.G. *Planning, Design, and Analysis of Tailings Dams*; BiTech Publishers: Vancouver, BC, Canada, 1990.
23. International Commission on Large Dams. *Tailings Dams: Risk of Dangerous Occurrences, Lessons Learnt from Practical Experiences*; ICOLD Bulletin 121; International Commission on Large Dams: Paris, France, 2001.
24. Rico, M.; Benito, G.; Salgueiro, A.R.; Díez-Herrero, A.; Pereira, H.G. Reported Tailings Dam Failures: A Review of the European Incidents in the Worldwide Context. *J. Hazard. Mater.* **2008**, *152*, 846–852. [CrossRef]
25. *GB/T 50123-2019*; Standard for Geotechnical Testing Method. Ministry of Housing and Urban-Rural Development of the People's Republic of China: Beijing, China; China Planning Press: Beijing, China, 2019.
26. *GB 50863-2013*; Code for Design of Tailings Facilities. Ministry of Housing and Urban-Rural Development of the People's Republic of China: Beijing, China; China Planning Press: Beijing, China, 2013.
27. Das, B.M.; Sobhan, K. *Principles of Geotechnical Engineering*, 9th ed.; Cengage Learning: Boston, MA, USA, 2018.
28. *ASTM D6913/D6913M-17*; Standard Test Methods for Particle-Size Distribution Gradation of Soils Using Sieve Analysis. ASTM International: West Conshohocken, PA, USA, 2017.
29. *ASTM D7928-21*; Standard Test Method for Particle-Size Distribution Gradation of Fine-Grained Soils Using the Sedimentation Hydrometer Analysis. ASTM International: West Conshohocken, PA, USA, 2021.
30. Wang, D.; Zhang, Q.; Chen, Q.; Qi, C.; Feng, Y.; Xiao, C. Temperature Variation Characteristics in Flocculation Settlement of Tailings and Its Mechanism. *Int. J. Miner. Metall. Mater.* **2020**, *27*, 1438–1448. [CrossRef]
31. Zheng, D.; Song, W.D.; Tan, Y.Y.; Cao, S.; Yang, Z.L.; Sun, L.J. Fractal and Microscopic Quantitative Characterization of Unclassified Tailings Flocs. *Int. J. Miner. Metall. Mater.* **2021**, *28*, 1429–1439. [CrossRef]
32. Been, K.; Sills, G.C. Self-Weight Consolidation of Soft Soils: An Experimental and Theoretical Study. *Géotechnique* **1981**, *31*, 519–535. [CrossRef]
33. Gibson, R.E.; England, G.L.; Hussey, M.J.L. The Theory of One-Dimensional Consolidation of Saturated Clays. I. Finite Non-Linear Consolidation of Thin Homogeneous Layers. *Géotechnique* **1967**, *17*, 261–273. [CrossRef]
34. Quezada, G.R.; Ramos, J.; Jeldres, R.I.; Robles, P.; Toledo, P.G. Analysis of the Flocculation Process of Fine Tailings Particles in Saltwater through a Population Balance Model. *Sep. Purif. Technol.* **2020**, *237*, 116319. [CrossRef]
35. Qi, C.; Fourie, A. Cemented Paste Backfill for Mineral Tailings Management: Review and Future Perspectives. *Miner. Eng.* **2019**, *144*, 106025. [CrossRef]

36. Tiller, F.M. Revision of Kynch Sedimentation Theory. *AIChE J.* **1981**, *27*, 823–829. [CrossRef]
37. Concha, F.; Bürger, R. A Century of Research in Sedimentation and Thickening. *KONA Powder Part. J.* **2002**, *20*, 38–70. [CrossRef]
38. Derjaguin, B.V.; Landau, L.D. Theory of the Stability of Strongly Charged Lyophobic Sols and of the Adhesion of Strongly Charged Particles in Solutions of Electrolytes. *Acta Physicochim. URSS* **1941**, *14*, 633–662.
39. Verwey, E.J.W.; Overbeek, J.T.G. *Theory of the Stability of Lyophobic Colloids*; Elsevier: Amsterdam, The Netherlands, 1948.
40. Hunter, R.J. *Zeta Potential in Colloid Science: Principles and Applications*; Academic Press: London, UK, 1981.
41. Terzaghi, K.; Peck, R.B.; Mesri, G. *Soil Mechanics in Engineering Practice*, 3rd ed.; John Wiley & Sons: New York, NY, USA, 1996.
42. Mitchell, J.K.; Soga, K. *Fundamentals of Soil Behavior*, 3rd ed.; John Wiley & Sons: Hoboken, NJ, USA, 2005.
43. Maxey, M.R.; Riley, J.J. Equation of Motion for a Small Rigid Sphere in a Nonuniform Flow. *Phys. Fluids* **1983**, *26*, 883–889. [CrossRef]
44. Mollehuara-Canales, R.; Kozlovskaya, E.; Lunkka, J.P.; Moisio, K.; Pedretti, D. Non-Invasive Geophysical Imaging and Facies Analysis in Mining Tailings. *J. Appl. Geophys.* **2021**, *192*, 104402. [CrossRef]
45. Mollehuara-Canales, R.; Afonin, N.; Kozlovskaya, E.; Lunkka, J.P.; Pedretti, D. Leveraging Active-Source Seismic Data in Mining Tailings: Refraction and MASW Analysis, Elastic Parameters, and Hydrogeological Conditions. *Bull. Geol. Soc. Finl.* **2021**, *93*, 105–127. [CrossRef]

Disclaimer/Publisher's Note: The statements, opinions and data contained in all publications are solely those of the individual author(s) and contributor(s) and not of MDPI and/or the editor(s). MDPI and/or the editor(s) disclaim responsibility for any injury to people or property resulting from any ideas, methods, instructions or products referred to in the content.